

# NEOPT: AN OPTIMIZATION SUITE FOR THE AEROELASTIC PRELIMINARY DESIGN

F. Toffol<sup>1</sup>, S. Ricci<sup>1</sup>

<sup>1</sup> POLITECNICO DI MILANO, Department of Aerospace Science and Technology  
Milano, Italy

[francesco.toffol@polimi.it](mailto:francesco.toffol@polimi.it)

[sergio.ricci@polimi.it](mailto:sergio.ricci@polimi.it)

**Keywords:** preliminary and conceptual design, aeroelastic optimization, meta-model.

**Abstract:** The paper describes the new optimization feature of the NeoCASS suite, which allows to size a general wing box structure considering the aeroelastic effects. During the conceptual phase of the design the aircraft is represented by a stick model with steady/unsteady aerodynamics (VLM/DLM), a link between the stiffness and mass matrices of the 1D elements and the 3D world is provided by a meta-model of the wing box.

The optimization is performed considering the maneuvers which define the load envelope of the aircraft compliant with CS25 regulation, analytical constraints on failure and buckling of the components are imposed.

## 1 INTRODUCTION

Nowadays, the increasing interest towards the climate changes and the transport related pollution affects the aeronautic industry, demanding for greener and more environment friendly aircraft. A way to tackle this topic is to design more efficient structures reducing the penalty mass. As a drawback, the design of lightweight and flexible structures may imply the arise of aeroelastic undesired effects such as flutter, control surfaces inefficiency and reversal, divergency and many others. Identify the weaknesses of the project in the early design phase is crucial to avoid further mitigation action, which often translates into a penalty mass.

For this reason, the designer must adopt tools which provide sufficient fidelity since the early stages of the aircraft design, in order to reduce the risk of encountering problems in late design phases where applying changes is very expensive.

Moreover, the reduction of the uncertainty in the design process allows to cut the development time and cost.

Aiming at providing a tool to fill the gap between the sketch of an aircraft and its first structural model, almost ten years ago NeoCASS [1][2] was developed within the EU-FP7 SimSAC project [4]. Since 2012, NeoCASS became a standalone, open source project publicly available. In the last decade many studies reached a high-fidelity level in multi-disciplinary optimization field, coupling detailed FEM model with CFD solvers [5][6] and improve solution strategies [7]. Although recent works reduced the computational effort needed to perform an high-fidelity MDO coupled with highly parallel multi-core computers, the whole optimization time, mesh generation excluded, goes from hours to days [8].

Most of the recent MDO studies start from a reference FEM/CFD model or a baseline, which is improved to its optimal solution.

NeOPT aims to shorten the distance between the blank sheet and the detailed MDO, by improving the knowledge about the aircraft configuration and its structural behaviour in the early design phases without demanding excessive computational effort.

NeOPT stands for **NeoCASS OPTimization Toolbox**, it is developed in Matlab and it performs the optimization using the solvers available in NeoCASS.

In this phase of the design, the aircraft is represented by a stick model where the structural mass and stiffness distributions are obtained by simple analytical models [3] in an automatic way using GUESS, one of the main modules of NeoCASS.

Starting from this initial model, the description of the wing box through bar elements is improved by the usage of an analytical formulation, called meta-model. This formulation describes the beam element cross-section starting from a variable number of design variables, such as the thicknesses of the panels of the shape of the stiffeners or spar caps. The main advantage of using a meta-model is that it is possible to virtually increase the fidelity of the structural model without the use of a more detailed finite element mesh, making the structural model relationships fully analytical. Through the same model, it is possible to recover the stresses distribution on the beam cross-section, which is used to evaluate the failure and buckling indices thanks to an analytic formulation. The safety margins are used as constraints during the optimization, but they are not the only ones. Whichever response of the simulation is a potential constraint or objective, for example the wing tip deflection during cruise condition rather than the roll moment due to the aileron, used to evaluate the effectiveness of the control surface.

After the optimization is completed, a geometry module generates a detailed full 3D model of the wing box in Nastran format and transforms the internal forces of the stick model into external forces to apply at the detailed model. The mathematical description of the 3D model is exported in an IGES file or Catia product.

The advantage of this procedure is to know the link between the 3D model and the stick model, in this way each change applied on one model is automatically transferred to the other one. This feature can be used as a condensation process, where the result of an optimization carried out on a detailed model can be reduced to a stick model which is suitable for other application such as aeroelastic dynamic response or state space modelling inside the NeoCASS environment.

NeOPT natural position inside NeoCASS flow diagram is after the GUESS (Generic Unknown Estimator in Structural Sizing) module.

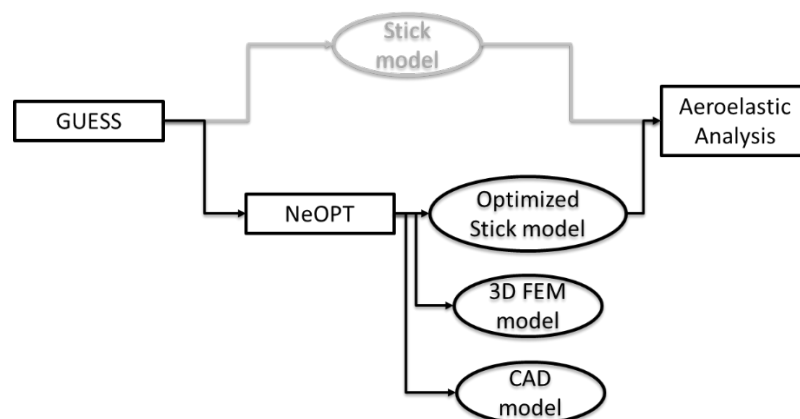


Figure 1: NeOPT in NeoCASS environment

GUESS provides a fully stress designed stick-model of the aircraft. The loads are obtained solving elastic trim problems, but they remain constant during the sizing of the aircraft components.

The result of the sizing is a stiffness distribution which carries the design loads without failure and buckling. The properties of the stick model are obtained starting from thickness distribution on the cross section, GUESS manages a symmetric wing box where upper and lower elements are equal (skins and stringers) while front and aft spar have the same thickness. The components are sized on each bar independently i.e. not patches subdivision is used spanwise. Indeed, due to the use of a simplified structural model, combined with the high number of load conditions to be applied, several limitations are applied during the initial sizing process by GUESS, i.e.: simple, fully stressed design; no composites structures available (just the so called black aluminum); no aeroelastic constraints.

The result of this sizing provides all the information necessary for the meta-modelling of the wing box such as front and rear spar position, rib and stringer pitch, initial values of wing box component thicknesses. In this view, NeOPT can be seen as a post-processor of GUESS results with a lot of improved capability in terms of structural model fidelity and capability to use any of the solvers available in NeoCASS. For sake of space available, in this paper an optimization using only the trim solver will be presented.

## 2 META-MODEL FORMULATION

### 2.1 Wing box description

The wing box is described by geometric dimensions, the height and the chord of the wing box are not used as design variables and are fixed. Other values that are not involved in the optimization are the stringer pitch and the rib pitch. All those parameters are user-defined and can be modified before the optimization.

A typical wing section is simplified to a rectangular section and it is described with a maximum of 10 variables, as illustrated in Figure 2. The typified wing box is made of T-shaped stringer, L-shaped spar caps, skin and spar web panels. The most general section uses 10 independent variables which are the thickness of upper and lower skin panels, the thickness of upper and lower stringer, the thickness of front and aft spar web and the thickness of each spar cap.

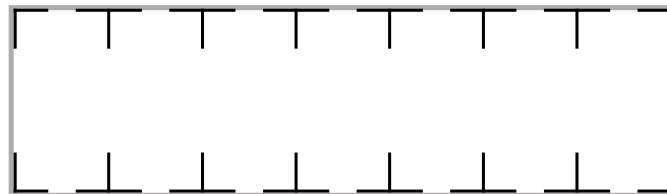


Figure 2: Rectangular wing box used in NeOPT

The T and L cross section are described by their thickness, their height and width are obtained by scaling the thickness by coefficients which do not vary during the optimization (Figure 3), but can be modified by the user.

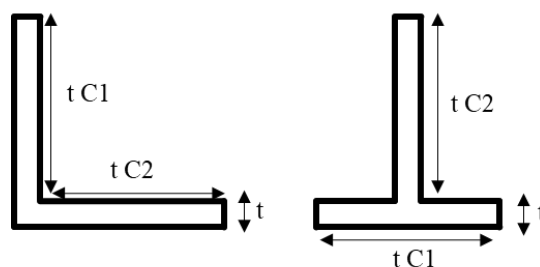


Figure 3: L-shaped and T-Shaped elements description

In NeOPT the user can reduce the number of variables on the cross section by imposing an equality constraint between the spar cap thickness, in order to have 7 variables. A further simplification can be made imposing the equality constraint between upper and lower panel thickness, front and rear spar web thickness, upper and lower stringer thickness. The last simplification leads to a section with only four variables and perfectly symmetric. In the last case the shear center, neutral axis and nodal lines are coincident.

The variables are not completely free to vary spanwise, a classical variable linking process across the ribs is implemented so the thicknesses values remain the same for a certain number of bays or patches. Figure 4 shows an example where the wing is divided in 5 patches.

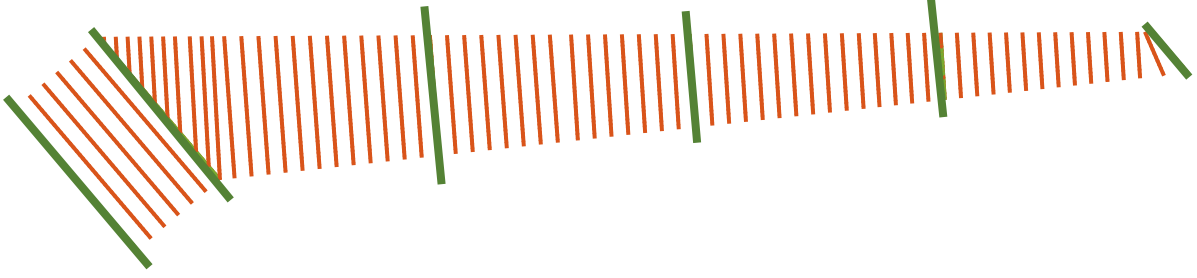


Figure 4: Example of spanwise patches subdivision

## 2.2 Stiffness properties

The cross-section stiffness properties derive from the material distribution on the cross section, the meta-model formulation allows to compute the beam stiffness matrix starting from geometrical values and material properties. The components of the wing box can be made of heterogenous materials, both isotropic and laminated composite. Thanks to the beam formulation adopted by NeoCASS [9], it is possible to provide the full 6x6 stiffness matrix for characterizing the cross-section behavior, both for coupling effects due to the materials and coupling effects due to offsets of the shear center and neutral axis from the nodal line. In Eq. (1) it is reported the stiffness matrix for an isotropic wing box, accounting the terms due to the offset of the shear centre ( $z_{sc}$ ,  $y_{sc}$ ) and neutral axis ( $z_{ea}$ ,  $y_{ea}$ ) from the nodes line.

$$K_{el} = \begin{bmatrix} EA_x & 0 & 0 & 0 & -EAz_{ea} & EAy_{ea} \\ 0 & GA_y & 0 & GA_y z_{sc} & 0 & 0 \\ 0 & 0 & GA_z & -GA_z y_{sc} & 0 & 0 \\ 0 & GA_z y_{sc} & -GA_y z_{sc} & GJ_t & 0 & 0 \\ -EAz_{ea} & 0 & 0 & 0 & EI_y & 0 \\ EAy_{ea} & 0 & 0 & 0 & 0 & EI_z \end{bmatrix} \quad (1)$$

The terms describing the axial and bending stiffnesses are computed analytically in Eq. (2), the stringers contribute to the bending stiffness only with their transport moment term, their local bending stiffness is neglected, as in Eq. (3). The properties are referred to the stick model nodes line.

$$EA_x = \sum_{i=1}^n E_i A_i ; \quad EI = \sum_{i=1}^n E_i I_i \quad (2)$$

$$I_{z \text{ str } i} = I_{z0i} + y_i^2 A_i \cong y_i^2 A_i \quad (3)$$

The method proposed in [10][11] provides the torsional stiffness and the shear center coordinates.

The assumptions made by the method are typically of semi-monocoque theory, i.e. the stringers withstand the loads due to the bending while the panels carry the shear stresses coming from shear forces and torque moment.

The external shape of the beam is maintained by closely spaced diaphragms extremely rigid in their plane and flexible normal to it. Considering the  $xy$  plane normal to the beam axis, the displacement of each point of the section can be described as an out-plane displacement along  $z$  axis Eq. (4) and an in-plane displacement along a curvilinear direction  $s$  Eq. (5). The three contribution in Eq. (4) are the axial displacement, the two terms due to the rotation around  $x$  and  $y$  axis and a warping term  $g$ . The convention for positive shear flow and the geometrical quantities used in the following equation are shown in Figure 5 a), while Figure 5 b) shows a warped section under pure shear load.

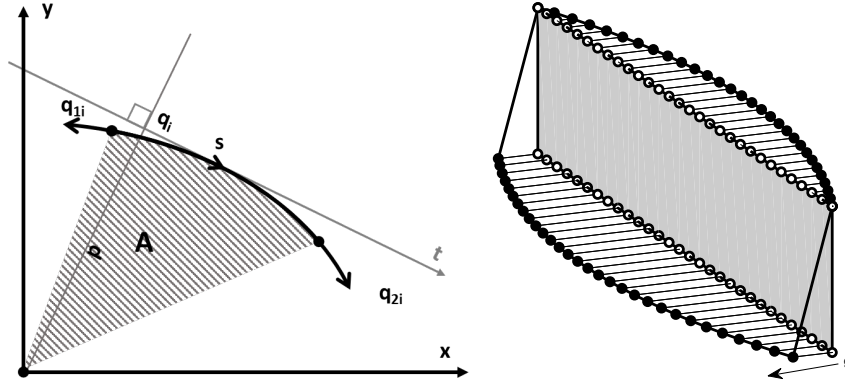


Figure 5: a) geometric quantities and shear flow positive direction on the beam cross-section b) section warping under pure shear load

$$w = w_0 - \frac{dv_0}{dz} y - \frac{du_0}{dz} x + g \quad (4)$$

$$v_t = u_0 \frac{dx}{ds} + v_0 \frac{dy}{ds} + p\theta \quad (5)$$

Being the shear strain defined as Eq. (6)

$$\gamma = \frac{\partial w}{\partial s} + \frac{\partial v_t}{\partial z} \quad (6)$$

And substituting Eq. (4) and Eq. (5) in Eq. (6), the shear strain becomes Eq. (7)

$$\gamma = \frac{dg}{ds} p \frac{d\theta}{dz} \quad (7)$$

Assuming constant thickness along the panel and integrating along the panel we obtain Eq. (8)

$$l\gamma = g_2 - g_1 + 2A \frac{d\theta}{dz} \quad (8)$$

In Eq. (8),  $l$  is the length of the panel and  $A$  is the area between the panel and the pole used for the moment evaluation, as shown in Figure 5.

The constant shear flow along the  $i$ -th panel is given by Eq. (9), where  $G_i$  is the shear module  $l_i$  the length,  $t_i$  the thickness of the panel and  $g$  is the warping value at the ends of the panel.

$$q_i = t_i \tau_i = t_i G_i \gamma_i = \frac{t_i G_i}{l_i} (g_{2i} - g_{1i} + 2A_i \dot{\theta}) \quad (9)$$

The positive direction for the curvilinear coordinate  $s$  is defined going from point 1 to point 2 and the shear flow is positive when exiting the panel, hence the flow in point 2 is the value obtained in Eq. (9), while the flow in point 1 is -Eq. (9). Moreover, the moment around the reference pole is defined in Eq. (10).

$$M_{oi} = 2A_i q_i \quad (10)$$

Combining Eq. (9) and Eq. (10), for the  $i$ -th panel we obtain Eq.(11).

$$\begin{bmatrix} q_{1i} \\ q_{2i} \\ M_{oi} \end{bmatrix} = \frac{G_i t_i}{l_i} \begin{bmatrix} 1 & -1 & -2A_i \\ -1 & 1 & 2A_i \\ -2A_i & 2A_i & 4A_i^2 \end{bmatrix} \begin{bmatrix} g_{1i} \\ g_{2i} \\ \dot{\theta} \end{bmatrix} \quad (11)$$

It is possible to assemble FEM-like system where the unknowns are the warping and the torsion of the section and the right-hand side term is made of the shear flow. The last step before solving the system is the assembly of the RHS term. Eq. (12) describes the axial load acting along a stringer

$$N_i = \frac{T_z}{A} A_i + \frac{M_x}{J_{xx}} y_i A_i - \frac{M_y}{J_{yy}} x_i A_i = \frac{T_z}{A} A_i + \frac{M_x}{J_{xx}} S_{xi} - \frac{M_y}{J_{yy}} S_{yi} \quad (12)$$

Neglecting the axial load, being the shear flow entering in the stringer equal and opposite to the variation of the axial load along the stringer and the shear force the derivative of the moment, we obtain Eq. (13).

$$q_i = -\frac{dN_i}{dz} = \frac{T_y S_{xi}}{J_{xx}} + \frac{T_x S_{yi}}{J_{yy}} \quad (13)$$

Now it is possible to assemble the system and its RHS term Eq.(14).

$$[K]\{u\} = \{P\} \quad (14)$$

The system in Eq. (14) is singular because we only have  $n-1$  independent equations. The warping of the section is defined unless a constant value used as reference, by placing this constant equal to zero, it is possible to delete a row and the corresponding column in order to avoid singularities. Once obtained the warping and the torsion of the section, shear stress is recovered using Eq. (9).

Solving Eq. (14) for  $T_y=1$ ,  $T_x=1$  and  $M_z=1$  distinctly, it is possible to compute the torsional stiffness and the coordinated of the shear center of the section.

The number of equations in Eq. (14) is equal to the number of stringers +1, adding one or more mid-spar in the section does not change the size of the system. This allows to analyze over determined sections with multiple cell both in terms of stiffness and shear flows.

### 2.3 Stress recovery and failure index

Solving the same system described in the previous section with the application of the internal forces instead of the unity forces lead to the shear stress due to external loads.

The strains due to the axial and bending deformation are recovered on the cross section through kinematic hypothesis shown in Eq. (15) and the axial stress is obtained multiplying the strain by the elastic modulus.

$$\varepsilon = \frac{N}{EA} - \frac{M_z}{EI_z}y + \frac{M_y}{EI_y}z \quad (15)$$

It is now possible to compute the failure index of the components, stringers and spar caps withstands only the axial stress while the skin panels and spar webs withstand axial and transverse shear. Von Mises's criterion is used for the isotropic material Eq. (16) and Tsai-Hill criterion is used for the composite materials Eq. (20). If the material is composite or made of multiple layer, the stress must be rotated in the material direction for each ply, according with Eq. (17)

$$FI_{VM} = \frac{\sigma_{yield}}{\sigma_{VM}} - 1, \text{ where } \sigma_{VM} = \sqrt{\sigma_{axial}^2 + 3\tau^2} \quad (16)$$

$$\begin{bmatrix} \sigma_1 \\ \sigma_2 \\ \tau_{12} \end{bmatrix} = Q_i A R A^{-1} Q^{-1} \begin{bmatrix} \sigma_{axial} \\ 0 \\ \tau \end{bmatrix} \quad (17)$$

In Eq. (17)  $Q_i$  is the 3x3  $i$ -th ply stiffness matrix for plane stress state,  $A$  is the transformation matrix in Eq. (18),  $R$  is the rotation matrix between laminate axis and ply axis Eq. (19),  $Q$  is the 3x3 laminate stiffness matrix for plane stress state and  $\alpha_i$  is the orientation of the  $i$ -th ply.  $X$ ,  $Y$  and  $S_{12}$  are the tension and shear limits for the ply.

$$A = \begin{bmatrix} 1 & & \\ & 1 & \\ & & 2 \end{bmatrix} \quad (18)$$

$$R = \begin{bmatrix} \cos^2\alpha_i & \sin^2\alpha_i & 2 \sin\alpha_i \cos\alpha_i \\ \sin^2\alpha_i & \cos^2\alpha_i & -2 \sin\alpha_i \cos\alpha_i \\ -2 \sin\alpha_i \cos\alpha_i & 2 \sin\alpha_i \cos\alpha_i & \cos^2\alpha_i - \sin^2\alpha_i \end{bmatrix} \quad (19)$$

$$FI_{TH} = 1 - \left( \frac{\sigma_1^2}{X} + \frac{\sigma_2^2}{Y} - \frac{\sigma_1\sigma_2}{X^2} + \frac{\tau_{12}^2}{S_{12}} \right) \quad (20)$$

The failure indices obtained are used as constraints during the optimization. The criteria are non-linear, but the stresses are recovered in a linear manner hence it is possible to multiply the internal forces by safety factor, typically 1.5, before the FI computation.

### 2.4 Buckling evaluation

Following the approach described in [12][13], it is possible to evaluate the buckling safety margin through an analytical formulation.

The approach works with the stiffness matrix of the plane element and it is developed for composite materials, but it is suitable even for the isotropic material. The critical  $N_{cr}$  value for

each load condition (axial, shear and bending) is given by an equation containing the terms of the D matrix in Eq. (21), which is the bending stiffness sub-matrix.

$$\begin{Bmatrix} N \\ M \end{Bmatrix} = \begin{bmatrix} A & B \\ B & D \end{bmatrix} \begin{Bmatrix} \varepsilon_0 \\ k \end{Bmatrix} \quad (21)$$

Buckling criteria adopted are non-linear, for this reason the loads are multiplied by a safety factor ( $sf=1.5$ ) before the criteria application.

The first buckling mechanism considered is the instability of the skin panel between two stringers and two ribs. The axial load and traverse shear act on the panel edges and the safety margin SM is obtained as described in Eq. (22).

$$SM = 1 - \frac{-N_x}{N_{cr x}} - \frac{|N_{xy}|}{N_{cr xy}} \quad (22)$$

In a similar fashion way, it is obtained the safety margin for the web of the spars, in this case the interaction formula Eq. (22) is enriched with the term due to the bending, becoming Eq. (23).

$$SM = 1 - \frac{-N_x}{N_{cr x}} - \frac{|N_{xy}|}{N_{cr xy}} - \frac{N_b}{N_{b cr}} \quad (23)$$

The buckling of the web of the T-shaped stringer is considered following [12], the stringer is loaded with an axial load and the safety margin is evaluated as shown in Eq. (24).

$$SM = 1 - \frac{-N_x}{N_{cr x}} \quad (24)$$

The last buckling mechanism considered is the instability of the stiffened panel between two consecutive ribs and two spars. The interaction formula considered is Eq. (22), but the critical values are computed accounting the effect of the stringer.

### 3 OPTIMIZER

NeoCASS is entirely developed in Matlab, hence the natural way to perform an optimization is to exploit the Matlab Optimization Toolbox [14]. NeOPT uses the *fmincon* function which finds the minimum of constrained nonlinear multivariable function.

The optimization problem is posed in the form of Eq. (25), where the objective function  $f(x)$  must be minimized satisfying a set of inequality constraints  $g(x)$ , with the variables bounded by upper and lower limits.

$$\min_x f(x) \text{ s. t. } x \in \mathcal{S}; \mathcal{S}: \{x \in \mathbb{R}^n \text{ s. t. } g(x) \leq \mathbf{0} \cap x_{lb} \leq x \leq x_{ub}\} \quad (25)$$

This built-in optimizer is gradient based and computes the gradient by finite differences when it is not provided. Gradient is evaluated exploiting the Matlab Parallel Computing Toolbox. The objective function can be whichever result of the solver used, or a combination of them. The most common single-objective function used in wing structural optimization is the mass, but other responses can be optimized. For examples NeOPT can be used for wing jig shape computation or the optimization of the aerodynamic derivatives.



NeOPT uses the solvers available in NeoCASS (static, modal analysis, aeroelastic trim, aeroelastic dynamic response, flutter computation) to calculate the aero structural responses to be used either as objectives or constraints.

Multiple trim cases or other aeroelastic analyses can be considered together during the optimization. For example, it is important to consider the entire load envelope when performing an aeroelastic sizing, hence it must be considered all the most critical maneuvers.

The standard mode of NeOPT uses the aforementioned structural constraints during the optimization, but as said for the objective function whichever response of the model can be used as additional constraint. An example can be the effectiveness of the aileron: when optimizing slender and flexible wing, the effectiveness of the control surface can be deteriorated. Constraining the roll moment due to aileron deflection to be higher than a certain value can avoid effectiveness reduction.

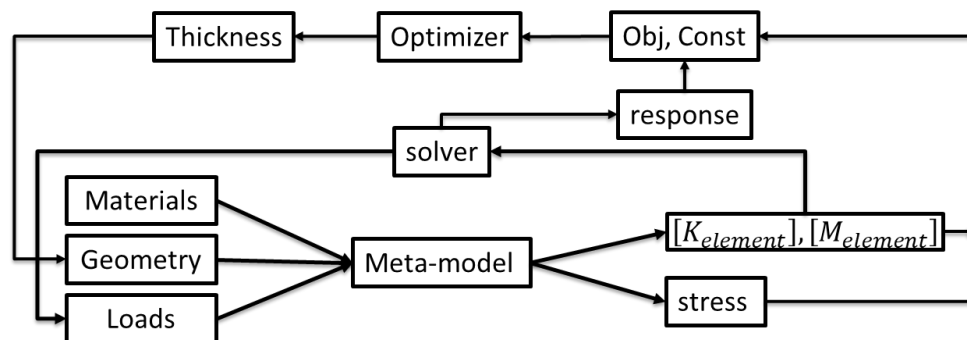


Figure 6: Optimization loop

Before starting the optimization, some preliminary operations are performed. The identification of the wing box dimension in terms of chord and height, the link between the variable both on the section and spanwise.

Aerodynamic matrices are computed for each Mach number considered in the envelope and stored at the beginning of the procedure, then they are called by the trim solver during the optimization. The same thing can be done during dynamic aeroelastic optimization or when the flutter constraint is activated. The DLM aerodynamic matrices are computed only once before starting the optimization. The modal shapes, affected by the changes in stiffness and mass matrices, is updated at each iteration and it is used to project the structural and aerodynamic matrices over the modal basis.

The initial value of the optimization is the result of the GUESS module.

As said previously, the solvers available are those implemented in NeoCASS, but thanks to the flexibility of NeOPT it can be interfaced with external solvers e.g. CFD.

The result of the optimization is the optimal thickness of each component that allows to satisfy the imposed constraints and minimize the objective function. The stick model provided as initial value is updated with the optimized properties and a detailed FEM model together with a CAD model are produced.

#### 4 GEOMETRIC MODULE

NeoCASS describes the wing box in terms of position of front and aft spar at given spanwise station, in the same position the airfoils are provided to. The geometry module, starting from these geometrical properties, identifies the external shape of the wing box. The surfaces are treated as a triangular mesh and through the method presented in [15] the intersection between surfaces is obtained. The pitch between two consecutive ribs is defined by the user, as well as the pitch between stringers. The ribs planes are normal to the nodal lines i.e. they are normal to the beam axis. After the intersection between ribs and wing box shape, the stringers

intersections are obtained. The stringers can be parallel to the front spar or to the mean axis of the wing box, if the wing box is tapered the stringers automatically interrupt on a rib. In the kink regions additional ribs are placed if necessary, their pitch is driven by the chordwise position of the stringer on the inner rib.

The resulting geometry is a cloud of points stored in a database which is processed and translated into a structured mesh of the wing box where the number of elements in chordwise, spanwise and thickness direction can be provided. The same database can be translated into an IGES file or a Catia product. When exporting IGES file, the rib sections are described as NURBS (Non-Uniform Rational B-Splines), this representation is suitable for shape parametrization in aerodynamic optimization problems [16][17]. The CAD model can be used for re-meshing some areas of the structure and performing more detailed analysis or to provide preliminary analysis for the integration of the wing sub-systems with the designed wing box.

The geometry module runs two time, the first one provides the geometrical information for the realization of the wing box meta-model, the second one takes place after optimization and produces the 3D FEM with the designed properties. Figure 7 shows an example of a CAD model and Figure 8 of a FEM mesh realized by the geometry module.

One of the most important characteristics of the geometry module is the connection between the stick-model and the 3D model through the meta-model: in this way each change in the properties of one of the two model is automatically reflected on the other model. This means that different level of optimization can be performed on different model without losing the relation between them. For example, a common problem of the optimization performed on high-fidelity 3D FEM model is the reduction of the wing-box to a stick model generally used for the load envelope evaluation, dynamic response analyses or state-space modelling for simulation and control purpose.

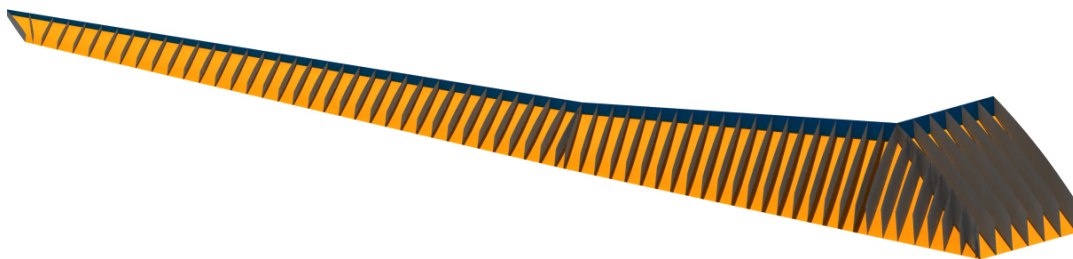


Figure 7: CAD model of a wing box

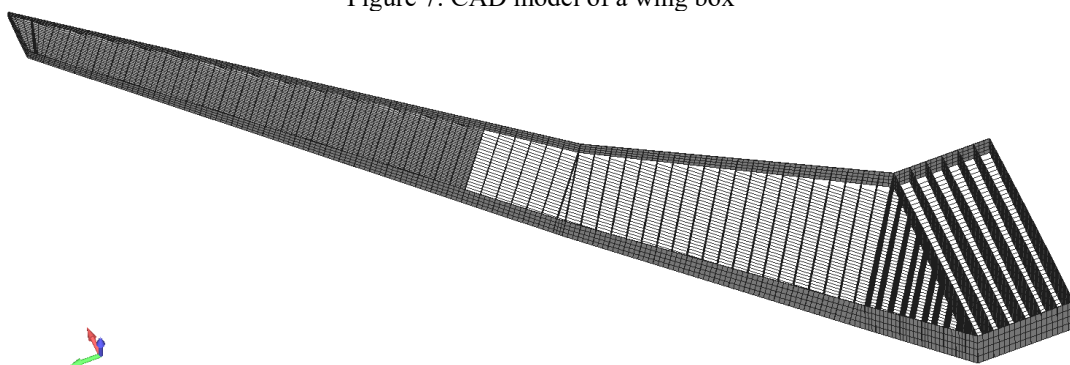


Figure 8: 3D FEM model of a wing box

Another feature of this module is the capability to transfer the loads from the stick model to the 3D model. This procedure calculates the forces and the moments which replicate the internal forces spanwise distribution, which is applied on the 3D model for reproducing a static case loading case with the load distribution coming from other aeroelastic analysis. This load set is typically used to perform stress analysis on the detailed 3D model.

Figure 9 shows how the internal forces obtained from a trim case on the aeroelastic stick model are reproduced by the application of a static load on the same model. Moreover, the deformed shapes obtained are the same for the two cases, as it is shown in Figure 10.

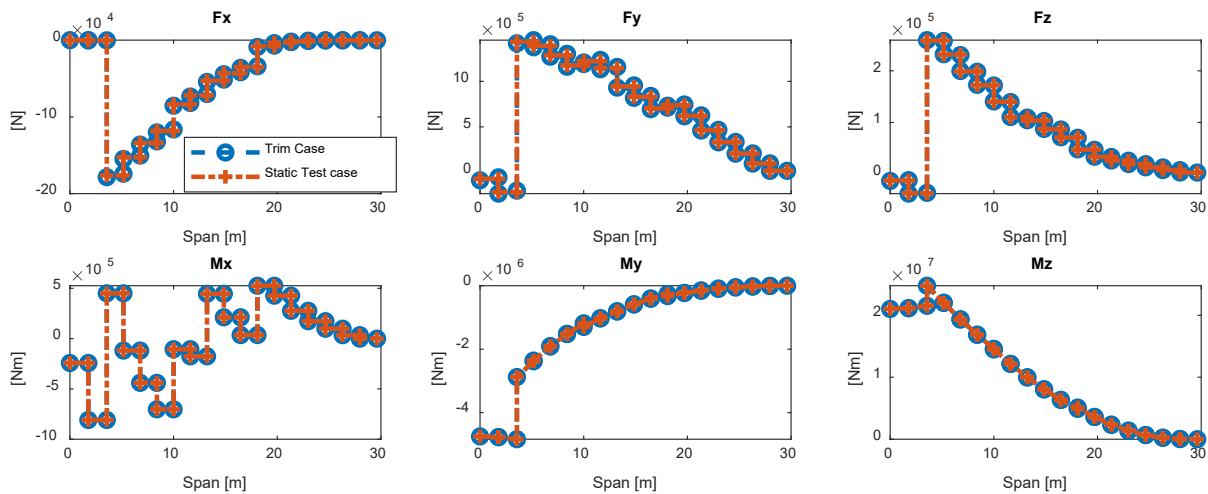


Figure 9: Internal forces obtained through trim analysis and static analysis in bar local coordinate system

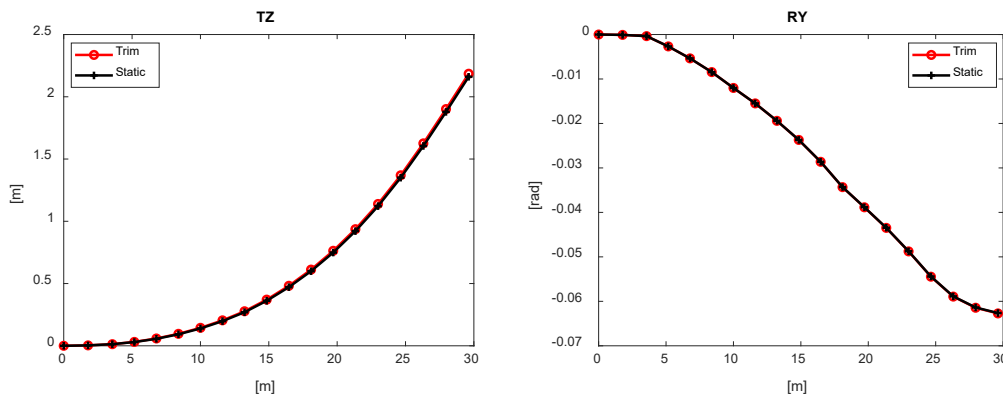


Figure 10: a) out plane z displacement and b) rotation around y axis in global coordinate system

## 5 META-MODEL VALIDATION

To validate the meta-model, the results obtained for static and modal simulation are compared with the ones coming from Nastran 3D FEM model. The comparison is carried out on the stress distribution (axial, transverse shear and Von Mises), on the deformed shape on the modal shapes and on the modal frequencies.

The comparison between the displacement and rotation provides an indication about the stiffness distribution, if the deformed shape of the two model is similar under the same static load also the stiffness distribution is equivalent. The second comparison performed is about the modal response of the two model, CrossMAC matrix provides information about the similarity of the modal shapes. Once assessed the quality of the stiffness distribution, the differences in modal frequencies provides indication about the mass distribution.

The test case is the rectangular wing box in Figure 11, which has a multiple cells section in the inner side and it is clamped on the root. The wing box is loaded with 6 independent load set, a force and a moment along x, y, z direction. The most significant cases are the application of a concentrated force along x axis (in plane load), along z axis (out plane load) and the application of a concentrated moment around y axis (torsion load). The next sections show the results of the static and modal analyses, the results will be discussed in 5.5.

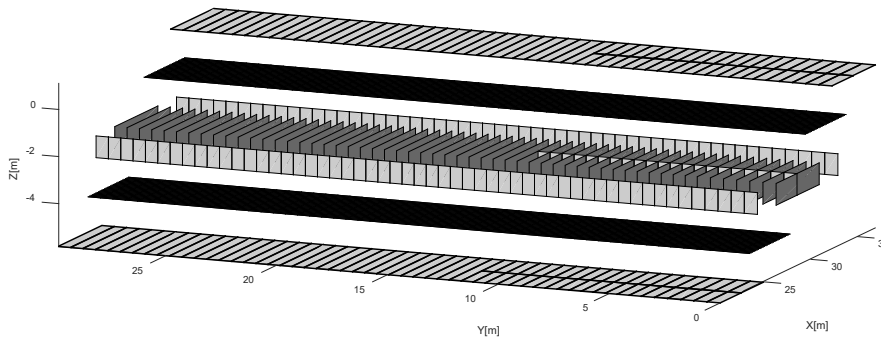


Figure 11: Rectangular wing box with multiple cell cross-section, two cells section in the inner part and one cell section in the outer part

### 5.1 In-plane tip load

The load acts along x direction and it is applied on the tip (y=30m). In Figure 12 it is reported the comparison between the stress distribution obtained with the detailed model (3D) and the meta-model (MM).

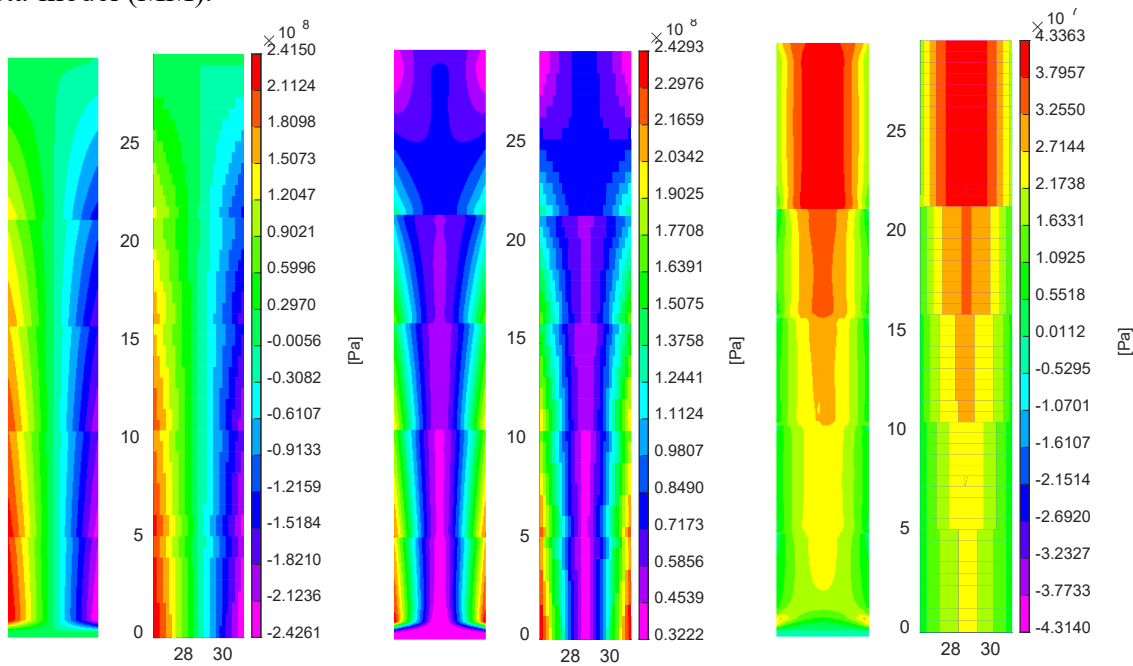


Figure 12: Upper skin stress distribution for in plane load. a) axial stress 3D, b) axial stress MM, c) Von Mises's stress 3D, d) Von Mises's stress MM, e) shear stress 3D, f) shear stress MM

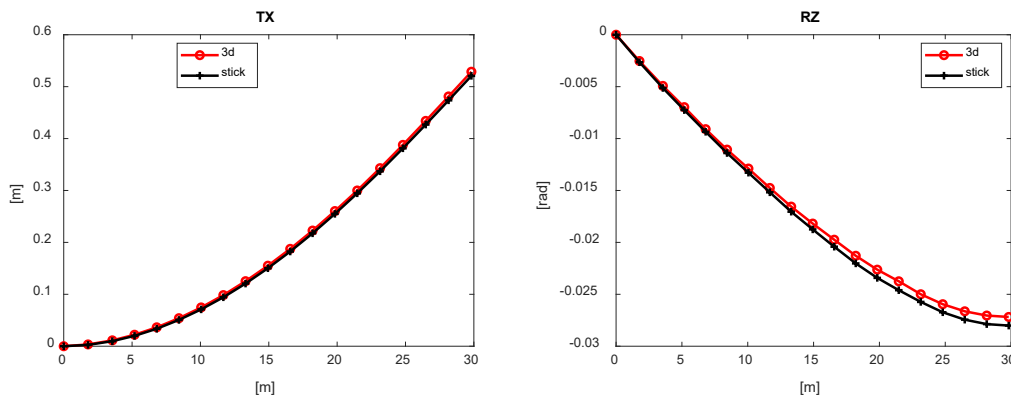


Figure 13: In plane load a) x displacement b) z rotation

### 5.2 Out of plane tip load

The load acts along z direction and it is applied on the tip (y=30m). In Figure 14 it is reported the comparison between the stress distribution obtained with the detailed model (3D) and the meta-model (MM)

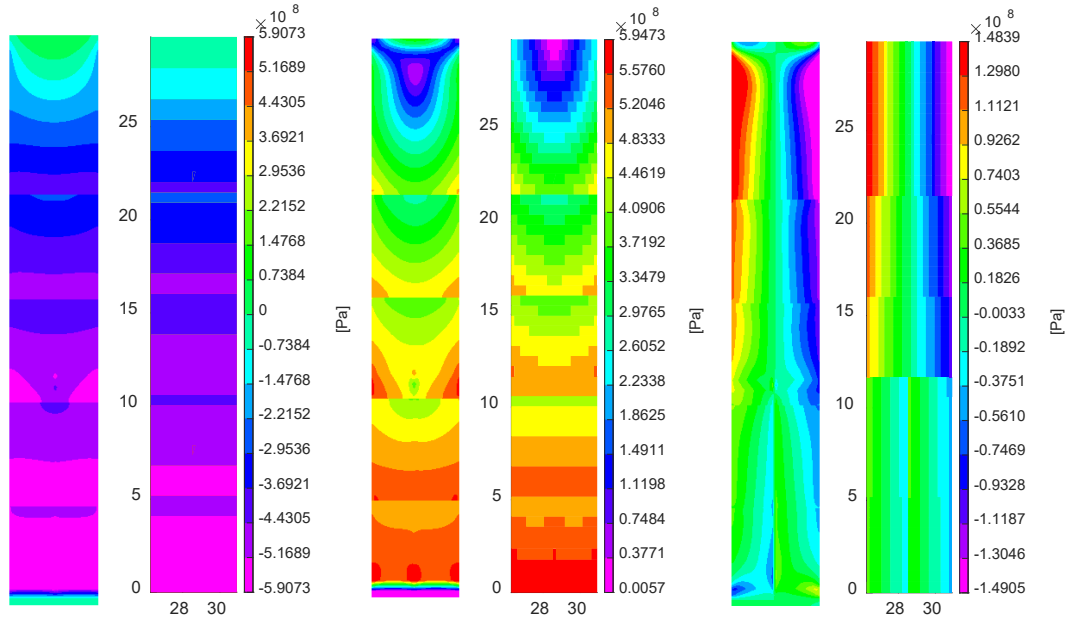


Figure 14:Upper skin stress distribution for out plane load. a) axial stress 3D, b) axial stress MM, c) Von Mises's stress 3D, d) Von Mises's stress MM, e) shear stress 3D, f) shear stress MM

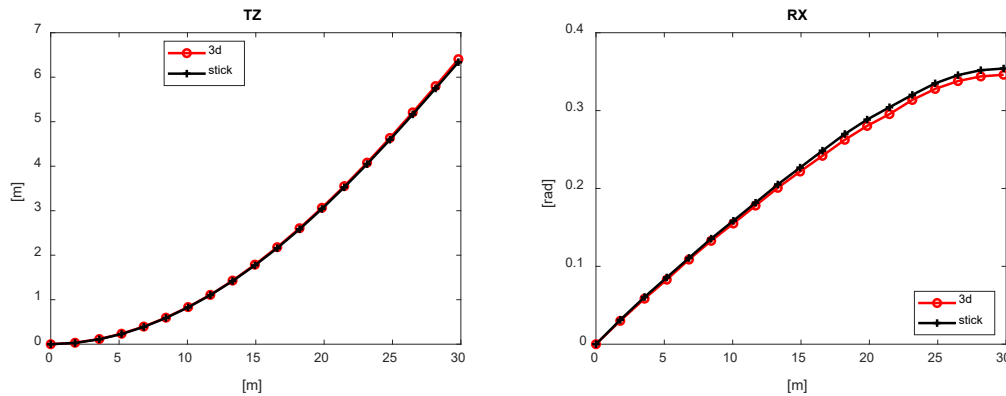


Figure 15: Out of plane load a) z displacement b) x rotation

### 5.3 Torsion load

The moment acts around y direction and it is applied on the tip (y=30m). In Figure 16 it is reported the comparison between the stress distribution obtained with the detailed model (3D) and the meta-model (MM)

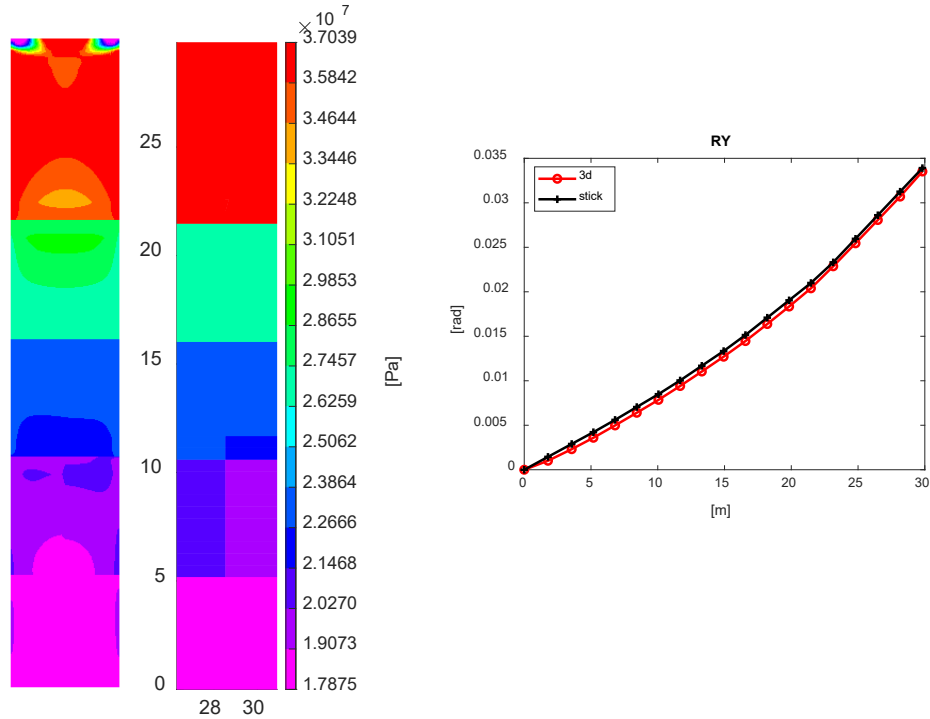


Figure 16: Upper skin stress distribution for torsional load. a) shear stress 3D, b) shear stress MM, c) rotation around y axis

#### 5.4 Modal analysis

The modal assurance criteria matrix (MAC) shown in Figure 18 considers only the displacements along x and z axes. To get information about the torsional modes the displacements are recovered on a set of nodes which have an offset from the nodal line, as shown in Figure 17. The wing is clamped at the root.

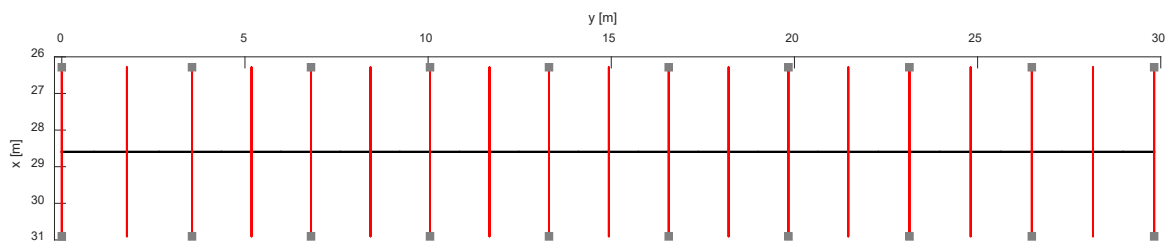


Figure 17: Grey square markers indicates the nodes where the displacements are recovered

The MAC matrix compares the modal shapes obtained for the two model and its values are obtained following Eq. (26).

$$MAC_{i,j} = \frac{|\Phi_i \Phi_j|^2}{(\Phi_i \Phi_i)(\Phi_j \Phi_j)} \quad (26)$$

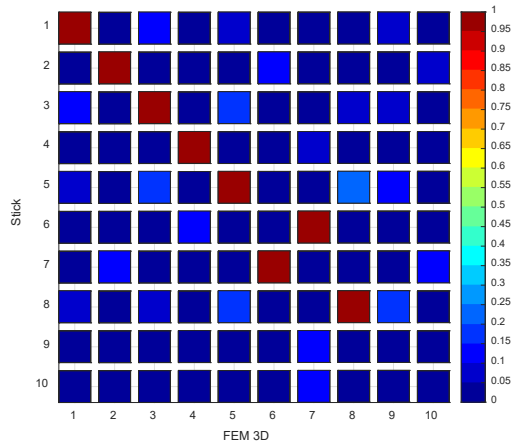


Figure 18: CrossMAC matrix for 3D and stick modal sets

Table 1: Modal frequencies comparison

Mode	Frequency stick [Hz]	Frequency 3D [Hz]	Error [%]
1	1.87	1.96	-4.67
2	6.51	6.63	-1.87
3	9.28	8.97	3.54
4	12.24	12.90	-5.08
5	24.18	20.58	17.50
6	31.41	27.82	12.91
7	32.01	33.18	-3.53
8	46.19	35.01	31.95
9	51.16	49.62	3.10
10	51.40	54.28	-5.31

## 5.5 Remarks on the meta-model validation

The stress comparisons between the distribution obtained for different load cases (Figure 12, Figure 14 and Figure 16) show that values recovered by the meta-model are similar to those obtained with FEM simulation, this is a relevant result because states the quality of the model used and its capability of recover stress information. The deformed shape of the two models are almost identical in terms of displacements and rotations (Figure 13, Figure 15, Figure 16). This states that the stiffness distribution of the two model is the same.

The modal assurance criterion indicates that the modal shapes are well matched, a switch between the 6<sup>th</sup> and the 7<sup>th</sup> mode id detected. The difference between the first 4 modal frequencies is lower than 5%, the error increases when the number of waves of the mode rises: e.g. on the first out-plane bending mode the error is -4.67% second out-plane bending mode the error is 17.5%. Since the stick model has a lumped masses formulation, the effect of the correct mass distribution is more emphasized at higher frequencies where the wave number of the mode increases.

The meta-model catches the macro-phenomena which we are interested in, allowing to perform an optimization on stick model with a limited number of nodes but it is still able to provide reliable information about the behavior of the 3D wing box. In the test case used the 3D FEM model has more than 16000 nodes while the stick model of the half wing counts only 19 nodes.

## 6 EXAMPLE

The main goal of this example is to proof that the whole procedure works, producing reliable results satisfying the constraint.

The objective is the wing box mass and the constraints are the safety margin on buckling and failure.

Starting from scratch, a B747-100 like stick model is realized following the template provided within NeoCASS and shown in Figure 19. The wing box is entirely made of aluminum. The initial sizing proposed by GUESS is performed on 29 trim conditions compliant with CS25 regulation. The trim envelope considers several maneuvers such as pull-up, push-down, sideslip for overswing angle and rudder deflection, abrupt roll due to aileron deflection, one engine inoperative at different speeds and altitudes. A load envelope in terms of bending/torsion and shear bending is drawn spanwise and only the worst conditions are used during the optimization, in this case the number of cases decreases from 29 to 17. Figure 19 b) shows an example of the enveloping maneuvers for a wing BAR element in terms of bending/torsion.

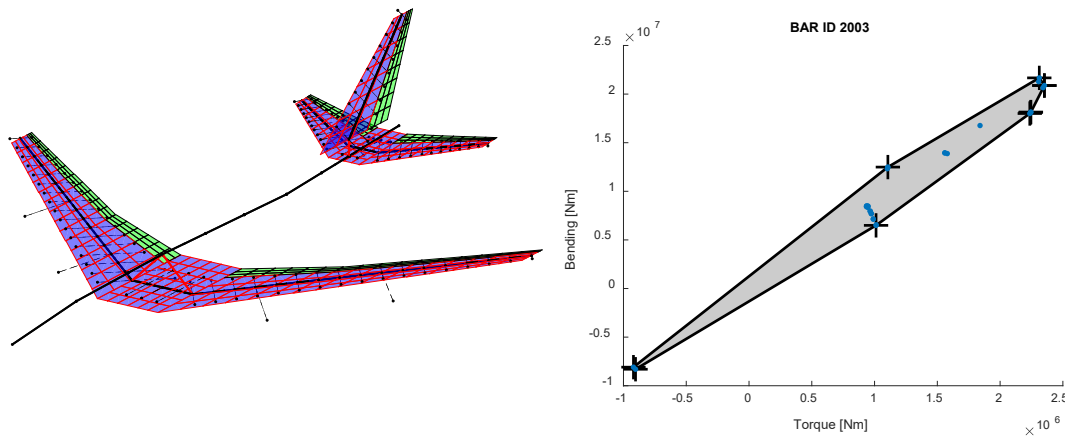


Figure 19: a) B747 stick model b) example of load envelope

The wing box is divided in 4 patches, and each patch has 7 variables, for a total of 28 variables. On each of the 64 bays, there are computed 18 constraints for each trim condition (10 failure and 8 buckling), for skin panels and stringers only the most critical element of each bay is considered. In this way the constraints matrix is made of 64 bays x 18 constraints=1152 rows and 18 trim cases columns. The constraint matrix is reduced to a 1152 x 1 vector by choosing only the most critical constraints among the trim conditions.

In the initial condition, the wing box (half wing) has a total mass of 18069 kg and it does not satisfy the constraint in several trim condition. After the optimization, the wing box mass decreases to 14080 kg which is 23% less. The optimized solution leads to a different material distribution, depicted in Figure 22 that translates in a more flexible wing both in terms of bending and torsion, as it is shown in Figure 23. The new structural solution changes the stress distribution, increasing the Von Mises's stress as Figure 21 shows.

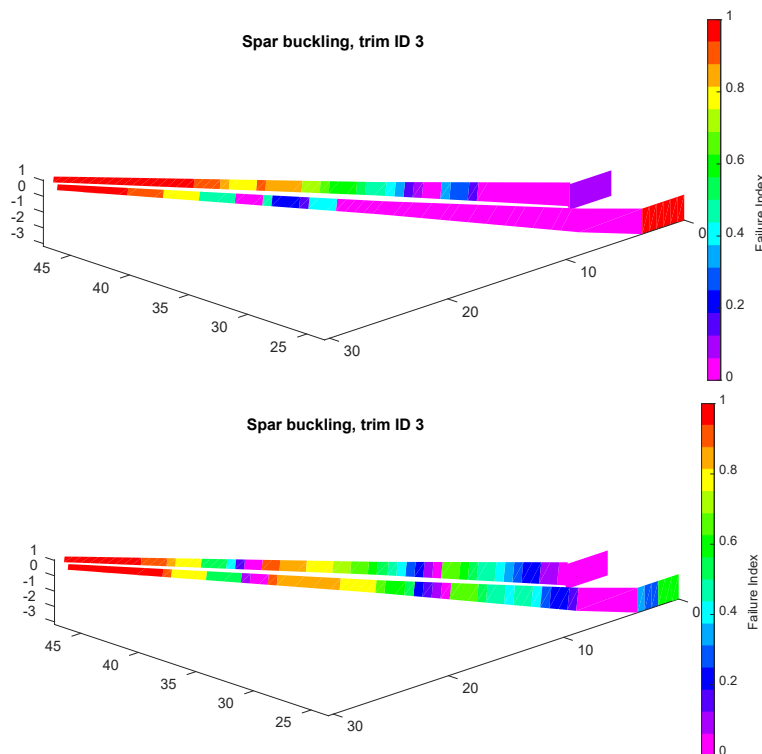


Figure 20: Buckling index a) before optimization b) after optimization



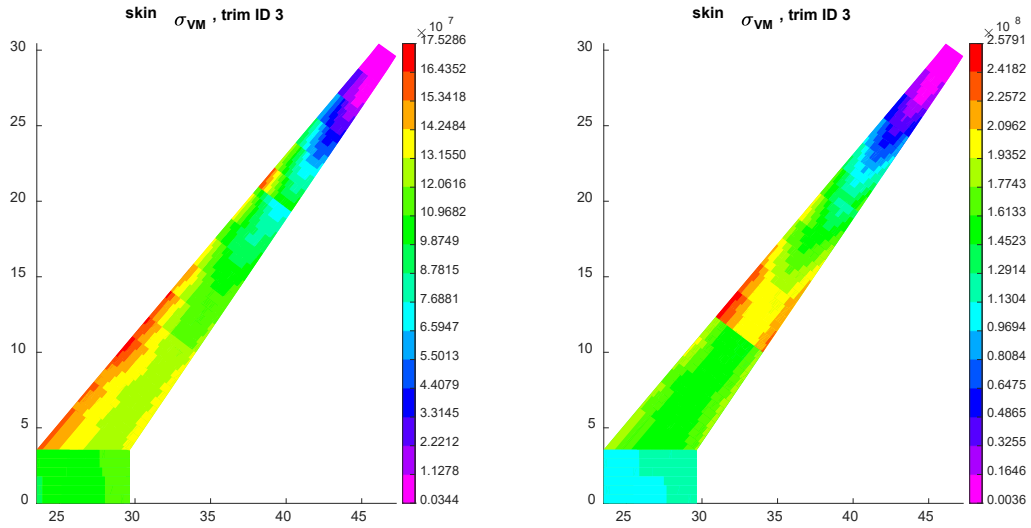


Figure 21: Von Mises's stress [Pa] distribution on upper panels a) before optimization b) after optimization

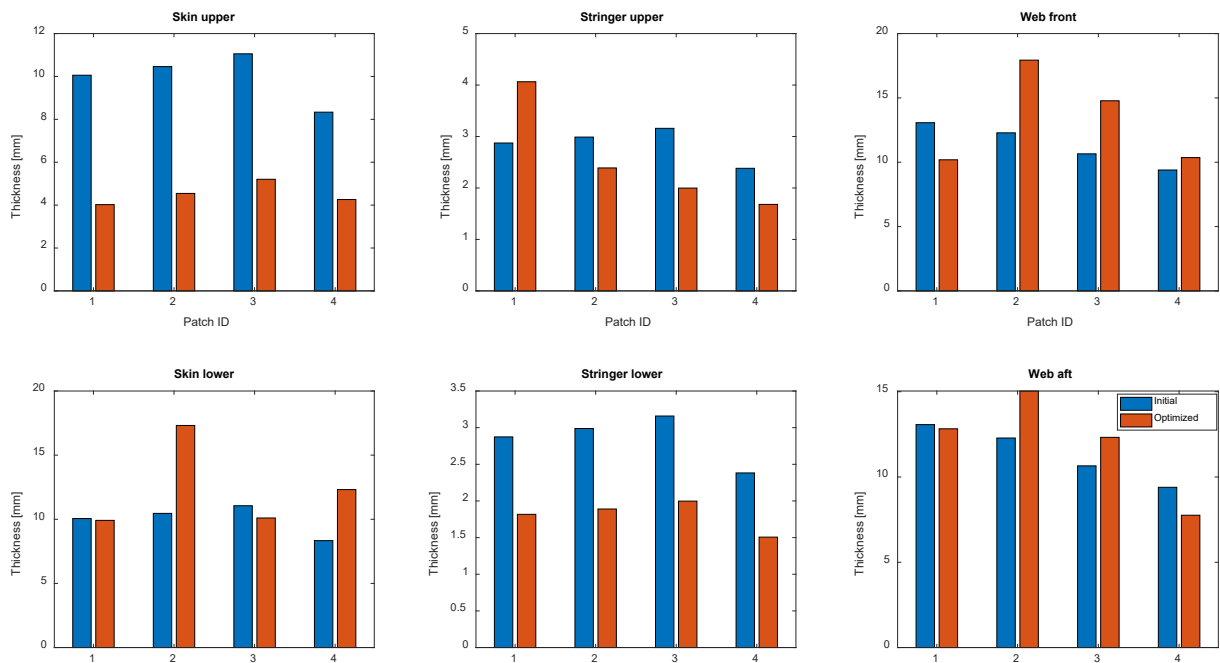


Figure 22: Design variables before and after the optimization

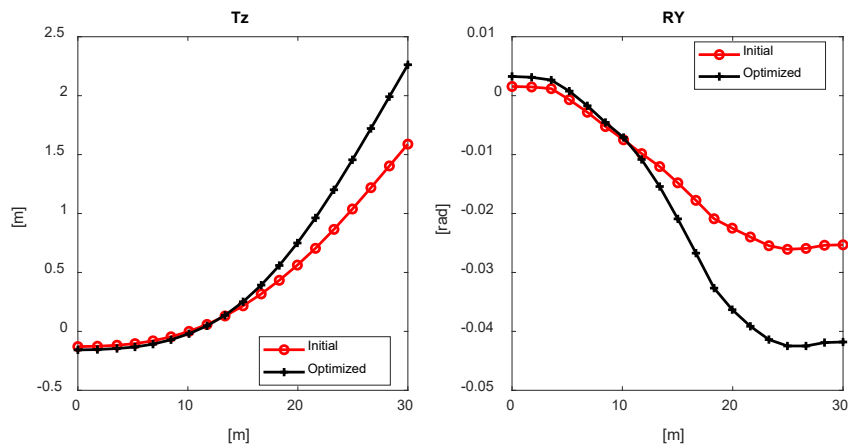


Figure 23: deformed shape for 2.5g pull up at dive speed a) out plane displacement b) y rotation

Figure 24 shows the importance of considering different trim maneuvers in the load envelope, the most critical condition varies spanwise and chordwise for the buckling of the skin panels. The inner part is dominated by pull-up and push-down but in the tip area the sideslope maneuver is critical.

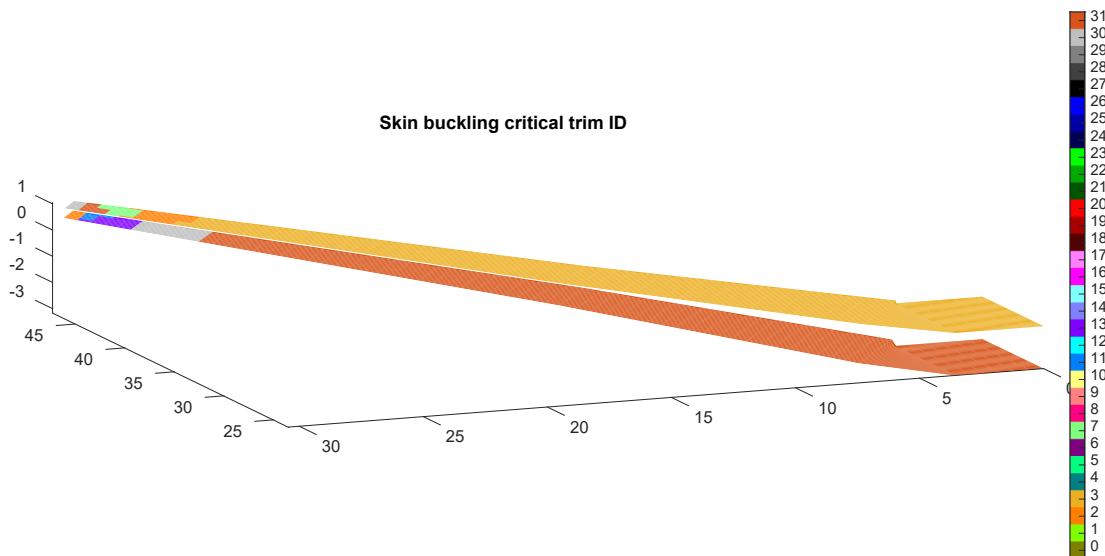


Figure 24: Most critical maneuver for skin panel buckling

## 7 CONCLUSIONS

This paper described the new optimization framework NeOPT included inside the NeoCASS suite.

Thanks to the optimization procedure it is possible to size a wing box satisfying strength and buckling constraints and taking into account a more detailed description of the wing box, including the presence of composite elements. The result of this procedure, performed in the conceptual design phase, can be the starting point for further detailed analyses and higher-fidelity optimization. Thanks to the adoption of an analytical model for the description of the cross section, any changes in the structure of the wing box can be applied to the stick model, which is suitable for certain application e.g. load envelope computing or state space representation of the aircraft.

The example proposed validates the procedure, minimizing the objective function with a feasible solution.

## 8 REFERENCES

- [1] Cavagna, L., Ricci, S., & Travaglini, L. (2011). NeoCASS: an integrated tool for structural sizing, aeroelastic analysis and MDO at conceptual design level. *Progress in Aerospace Sciences*, 47(8), 621-635.
- [2] Cavagna, L., Ricci, S., & Travaglini, L. (2010). Structural sizing and aeroelastic optimization in aircraft conceptual design using NeoCASS suite. In *13th AIAA/ISSMO Multidisciplinary Analysis Optimization Conference* (p. 9076).
- [3] Cavagna, L., Ricci, S., & Riccobene, L. (2009). A fast tool for structural sizing, aeroelastic analysis and optimization in aircraft conceptual design. In *50th AIAA/ASME/ASCE/AHS/ASC Structures, Structural Dynamics, and Materials Conference 17th AIAA/ASME/AHS Adaptive Structures Conference 11th AIAA No* (p. 2571).

- [4] Rizzi, A. (2011). *Modeling and simulating aircraft stability and control—the SimSAC project*. *Progress in Aerospace Sciences*, 47(8), 573-588.
- [5] Martins, J. R., Alonso, J. J., & Reuther, J. J. (2004). *High-fidelity aerostructural design optimization of a supersonic business jet*. *Journal of Aircraft*, 41(3), 523-530.
- [6] Lyu, Z., Kenway, G. K., & Martins, J. R. (2014). *Aerodynamic shape optimization investigations of the common research model wing benchmark*. *AIAA Journal*, 53(4), 968-985.
- [7] Mittelman, H. (2010) *Decision tree for optimization software*. Tech Rep, School of Mathematical and Statistical Sciences, Arizona State University. <http://plato.asu.edu/guide.html>
- [8] Kenway, G. K., & Martins, J. R. (2014). *Multipoint high-fidelity aerostructural optimization of a transport aircraft configuration*. *Journal of Aircraft*, 51(1), 144-160.
- [9] Ghiringhelli, G. L., Masarati, P., & Mantegazza, P. (2000). *Multibody implementation of finite volume C beams*. *AIAA journal*, 38(1), 131-138.
- [10] Giavotto, V. (1977) *Strutture aeronautiche*. Clup.
- [11] Mantegazza, P. (1977) *Analysis of semimonocoque beam sections by the displacement method*, *L'Aerotecnica Missili e Spazio*, pp. 179–182
- [12] Herencia, J. Enrique; Weaver, Paul M.; Friswell, Michael I. (2007) *Optimization of long anisotropic laminated fiber composite panels with T-shaped stiffeners*. *AIAA journal*, 2007, 45.10: 2497.
- [13] Weaver, Paul M.; Nemeth, Michael P. (2007) *Bounds on flexural properties and buckling response for symmetrically laminated composite plates*. *Journal of engineering mechanics*, 2007, 133.11: 1178-1191.
- [14] The Mathworks Inc., Optimization Toolbox User Guide, 2018
- [15] Möller, T. (1997). *A fast triangle-triangle intersection test*. *Journal of graphics tools*, 2(2), 25-30.
- [16] Samareh, J. (2004, August). *Aerodynamic shape optimization based on free-form deformation*. In 10th AIAA/ISSMO multidisciplinary analysis and optimization conference (p. 4630).
- [17] Samareh, J. A. (2001). *Survey of shape parameterization techniques for high-fidelity multidisciplinary shape optimization*. *AIAA journal*, 39(5), 877-884.

## COPYRIGHT STATEMENT

The authors confirm that they, and/or their company or organization, hold copyright on all of the original material included in this paper. The authors also confirm that they have obtained permission, from the copyright holder of any third party material included in this paper, to publish it as part of their paper. The authors confirm that they give permission, or have obtained permission from the copyright holder of this paper, for the publication and distribution of this paper as part of the IFASD-2019 proceedings or as individual off-prints from the proceedings.